



## ICTS Measurements of Single Grain Boundaries in ZnO:rare-earth Varistor

AKINORI TANAKA & KAZUO MUKAE

*Fuji Electric Corporate Research and Development Ltd., 2-2-1 Nagasaka, Yokosuka-shi, Kanagawa, 240-0194, Japan*

Submitted November 14, 1997; September 29, 1998; May 10, 1999

**Abstract.** Properties of single grain boundaries in ZnO:rare-earth varistors were examined by the isothermal capacitance transient spectroscopy (ICTS) method. Micro-electrodes prepared by photolithography were used for measuring the behavior of single junctions in ZnO varistors. From current-voltage measurements, it was found that the non-linear exponents of single junctions varied from 3 to 14. Interface state levels existed at 0.9 eV below the conduction band edge for every junction. On the other hand, the interface state density varied from junction to junction and the non-linearity was shown to increase with increasing interface state density.

**Keywords:** zinc oxide, varistor, ICTS, single junction, interface state

### Introduction

Zinc oxide varistors are known as electric surge absorbing devices [1]. Their non-linear current-voltage ( $I$ - $V$ ) characteristics originate from the double Schottky barrier formed at the ZnO grain boundaries [2–4]. Interface states at grain boundaries are supposed to be responsible for the formation of Schottky barriers. In order to clarify the properties of interface states, measurements on trap levels at ZnO grain boundaries were conducted by several groups of researchers [5–9]. Trap levels were detected by the capacitance transient method [5]. Deep level transient spectroscopy (DLTS [10]), proposed by Lang, was found suitable for characterizing defects in semiconductors and this method was subsequently applied to ZnO varistors. Shohata et al. and Nitayama et al. showed that bulk trap levels were located approximately 0.3 eV below the conduction band edge [6, 7]. Tsuda et al. showed that an interface state level existed at 1.03 eV below the conduction band edge [8]. However, the formation mechanism of interface states is not clear. Since the above measurements were performed on bulk samples, their results reflected the average characteristics of thousands of grain boundaries inside the sample.

In order to study ZnO grain boundaries further, direct measurements of single grain boundaries were attempted by several groups. They measured the current-voltage characteristics of single junctions in ZnO varistors [11–14]. According to their measurements, the threshold voltage of a single junction was found to be 3 V. However, there were few discussions on the correlation between a single junction's  $I$ - $V$  characteristics and its interface states. It is of great importance to correlate single junction's  $I$ - $V$  characteristics and interface state properties, because  $I$ - $V$  characteristics should be affected by interface states. Thus single junction measurement on interface states is necessary to characterize the varistor and its grain boundaries in detail. H. Wang et al. examined the ZnO single junction by DLTS [15]. However they didn't discuss the relation between  $I$ - $V$  characteristics and interface state levels.

In this study isothermal capacitance transient spectroscopy (ICTS [16]) was applied to single grain boundaries in Pr doped ZnO varistors. The ICTS method is one of the capacitance transient methods by which the interface state level and the capture cross section can be obtained as in DLTS measurements [17, 18]. The ICTS signal  $S(t)$  is defined by the following,

$$S(t) = t \frac{df(t)}{dt} \quad (1)$$

where  $f(t)$  is given by

$$f(t) = \left( \frac{1}{C(t)} - \frac{1}{C(\infty)} \right) \quad (2)$$

where  $C(t)$  is the junction capacitance at time  $t$  and  $C(\infty)$  is the steady state capacitance. Since a capacitance transient occurs by emission or capture of electrons at trap levels,  $f(t)$  is described by the following relation.

$$f(t) \propto \exp(-e_n t) \quad (3)$$

where  $e_n$  is the thermal emission rate of electrons at the trap level, which is given by

$$e_n = N_c \sigma_n \nu_{th} g^{-1} \exp(-E_{IS}/kT) \quad (4)$$

where  $N_c$  is the effective density of states in the conduction band,  $\sigma_n$  is the capture cross section,  $\nu_{th}$  is the thermal velocity, and  $g$  is the degeneracy,  $E_{IS}$  is the interface state level below the conduction band edge,  $k$  is the Boltzmann constant, and  $T$  is absolute temperature. From Eq. (1) and (3),  $S(t)$  has a peak value  $S_{\max}$  at  $e_n t = 1$ .

$$S_{\max} = - \frac{N_{IS}}{\varepsilon_s N_D A e} \quad (5)$$

where  $N_{IS}$  is the density of interface state,  $\varepsilon_s$  is permittivity of Zinc oxide,  $N_D$  is shallow donor concentration,  $A$  is the junction area, and  $e$  is natural logarithm. The interface state level,  $E_{IS}$ , and capture cross section,  $\sigma_n$ , are obtained from  $e_n$  measured at several temperatures. Since  $\sigma_n \times N_c$  is proportional to  $T^2$ , the activation energy  $E_{IS}$  of the interface state is obtained from the slope of an Arrhenius plot of  $\ln(e_n/T^2)$  and  $1000/T$ . Meanwhile the interface state density is obtained by the peak value of the ICTS spectrum using Eq. (5).

Single grain boundaries measurements were carried out using micro-electrodes formed by photolithography on the surface of the samples. These were used to examine the  $I$ - $V$  characteristics and interface state properties of single junctions in ZnO varistors.

## Experiment

Regent grade ZnO and  $\text{Co}_3\text{O}_4$  and high purity  $\text{P}_6\text{O}_{11}$  (99.9%) were used as starting materials. The sample composition was ZnO plus 0.5 at. %  $\text{Pr}_6\text{O}_{11}$ , and 2.0 at. %  $\text{Co}_3\text{O}_4$ . Powders were mixed for 20 h in a ball mill

with water and  $\text{ZrO}_2$  balls. The slurry was dried and pressed into pellets with a pressure of  $900 \text{ kg/cm}^2$ . Then pellets were sintered at  $1450^\circ\text{C}$  for 2 h in air and furnace-cooled. The samples obtained were 14 mm in diameter and 1.2 mm in thickness. Silver electrodes, 12 mm in diameter, were printed by screen printing on both sides of the samples and heat-treated at about  $600^\circ\text{C}$ . Then  $I$ - $V$ , capacitance-voltage, and ICTS measurements were carried out on these samples.

After bulk measurements, the silver electrodes were removed. Then the surface of the samples was polished using a polishing cloth and diamond paste as polishing media. The samples were then thermally etched at  $1050^\circ\text{C}$  for 1 h. This procedure made grain boundaries visible and relaxed the polishing damage to the surface. The photolithography technique was used to form micro-electrodes on the surface of each sample. Figure 1 shows the pattern of micro-electrodes. There are 72 pair of electrodes in the pattern. The tips of the electrodes are  $5 \mu\text{m}$  wide. The distance between a pair of electrodes is  $10 \mu\text{m}$ . Aluminum was used for the electrode material. The grain boundaries which crossed between a pair of micro-electrodes were confirmed by an optical microscope. Figure 2 shows an SEM photograph of a single junction and micro-electrodes.

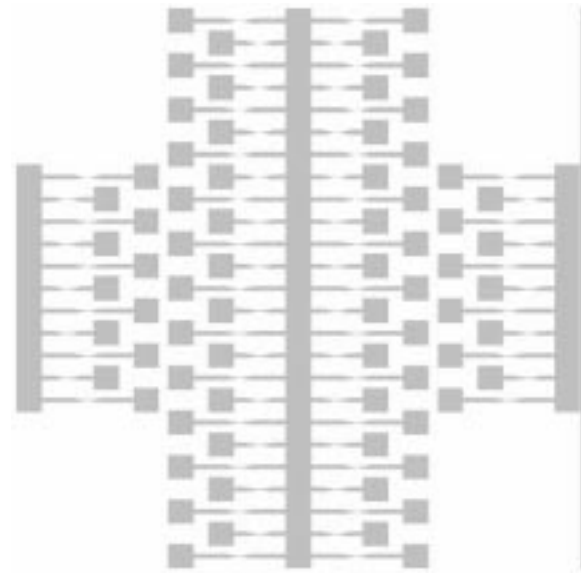


Fig. 1. Electrode pattern for single junction measurements.

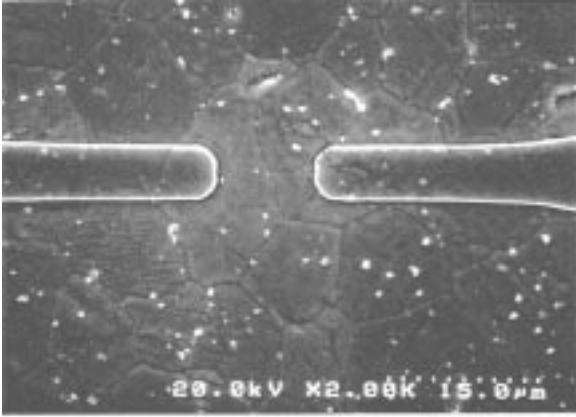


Fig. 2. SEM photograph of a single junction and micro-electrodes.

For single junction measurements, the sample was placed on the heater inside the sample box. The temperature was controlled by a temperature controller. Tungsten probes were used for electrical contacts.  $I$ - $V$  characteristics were measured by a curve tracer (TT-505 curve tracer, Iwatsu Electric Co., Ltd.). ICTS measurements were carried out with a capacitance meter (MI-401 DLTS test system, Sanwa musen) with a digital memory (DM-2350 digital memory, Iwatsu Electric Co., Ltd.). Figure 3 shows a block diagram of the ICTS measurement system. The applied voltage for a single junction was fixed to 1.5 V height and 10 s width for each measurement. The

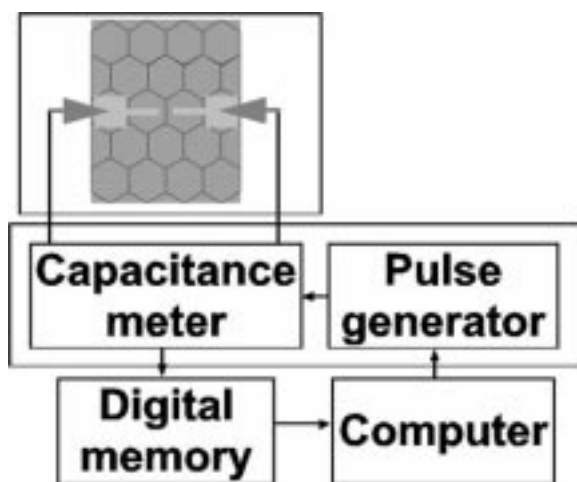


Fig. 3. Block diagram of the ICTS measurement system.

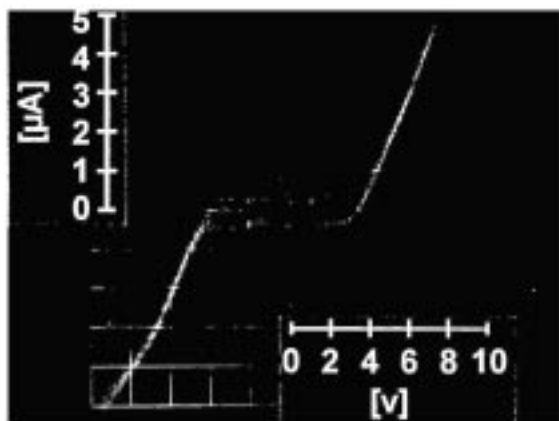
capacitance transient was measured after the pulse was removed. Capacitance data collected by the capacitance meter were stored in digital memory. Then the data were transferred to a computer and the spectrum was calculated. Measured temperatures were varied from 80 to 120°C in 10°C steps.

### Results and Discussion

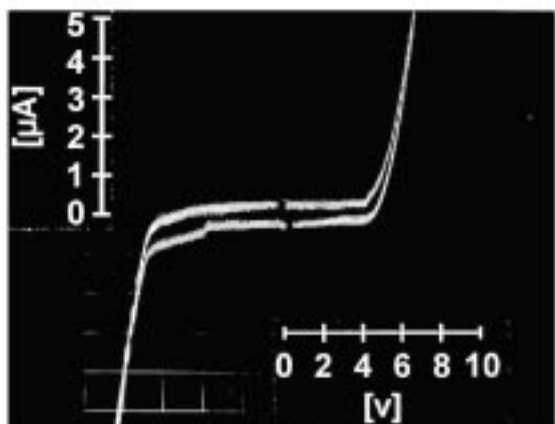
From bulk measurements, our samples' varistor breakdown voltage per 1 mm averaged 38.7 V/mm. The non-linear exponent  $\alpha$  defined as  $I = kV^\alpha$  obtained by  $V_{10\mu A}$  and  $V_{1mA}$ , was 8.6. This value is relatively low, since  $\alpha$  usually exceeds 50 for commercial varistors. This is due to the simple composition of the samples and the higher sintering temperature employed. High sintering temperatures were necessary, in order to large grains and thus larger junction capacitance thereby improving the S/N ratio of the ICTS spectrum. The donor density obtained by the capacitance-voltage method [19] was  $6.7 \times 10^{17} \text{ cm}^{-3}$ .

Figure 4 shows current-voltage characteristics for several single junctions. Their non-linearity varied from junction to junction and their non-linear exponents varied from 3 to 14. The corresponding coefficient of the sintered material,  $\alpha = 8.6$ , seems to be an average characteristic of these junctions' properties.

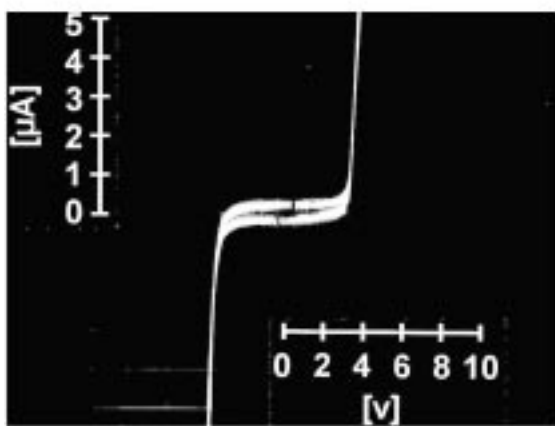
Figure 5 shows an example of the ICTS spectra obtained for a single grain boundary in a ZnO varistor. Only single peaks were observed and those peaks were shifted to shorter time with increasing temperature, since electron relaxation increases with temperature. Figure 6 shows an Arrhenius plot of  $\ln(e_n/T^2)$  vs. temperature. The interface state level and the capture cross section were obtained from the slope and the intercept, respectively. Table 1 shows the interface state parameters obtained by single junction ICTS measurements. The values are the average over 9 junctions. Table 2 shows individual characteristics of these 9 junctions. Parameters obtained by bulk measurement are also shown in Table 1. An interface state level was located at 0.9 eV below the conduction band edge. This result agrees with the literature value [8, 9] and was stable for every junction. On the other hand, the capture cross section and interface state density varied from junction to junction. The interface state density obtained by



(No. 1)



(No. 2)



(No. 3)

Fig. 4. I-V characteristics of several single junctions.

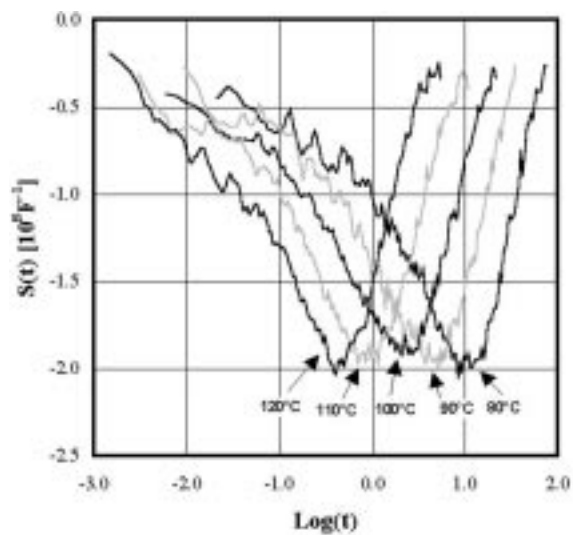


Fig. 5. ICTS spectra for a single junction.

single junction measurements was quite different from that obtained by bulk measurements. The value by the single junction method is two orders of magnitude lower than that by bulk measurements. This discrepancy comes from the effect of surrounding junctions, since their capacitances were added to that of the target single junction.

The *I-V* characteristics of single junctions could be explained by the property of interface states at single junctions. There are three principal factors—(1) donor density [ $N_D$ ]; (2) interface state level [ $E_{IS}$ ];

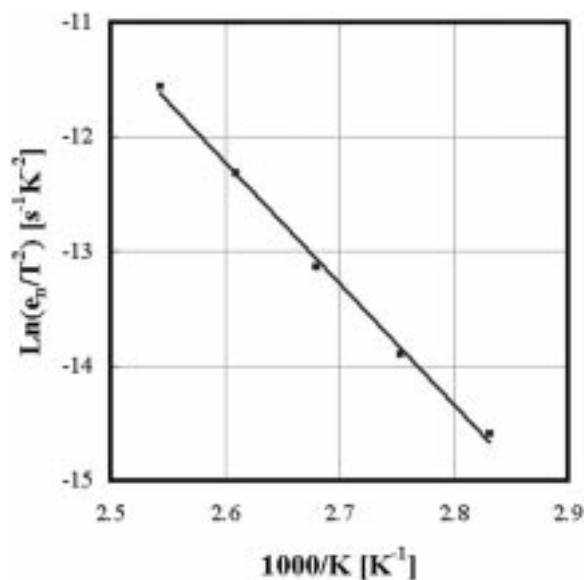


Fig. 6. Arrhenius plot of peak temperature and  $\ln(e_n/T^2)$ .

Table 1.

	Interface state level $E_{IS}$ [eV]	Capture cross section $\sigma$ [ $\text{cm}^2$ ]	Interface state density $N_{IS}$ [ $\text{cm}^{-2}$ ]
Bulk	0.80	$2.16 \times 10^{-16}$	8.9611
Single junction	0.91	$3.78 \times 10^{-14}$	$3.10 \times 10^9$

Table 2.

Junction	Interface state level [eV]	Capture cross section [ $\text{cm}^2$ ]	Interface state density [ $\text{cm}^{-2}$ ]	Non-linear Exponent
1	0.91	$2.1510^{-14}$	$3.7410^9$	4.5
2	0.87	$4.5110^{-15}$	$6.8610^9$	14.5
3	0.83	$1.7910^{-15}$	$5.0410^9$	6.8
4	0.94	$4.3110^{-14}$	$4.1510^9$	3.4
5	0.96	$6.9810^{-14}$	$1.6910^9$	2.8
6	0.84	$2.2510^{-15}$	$4.6110^9$	4.7
7	0.98	$1.5310^{-13}$	$2.0910^9$	2.9
8	0.96	$6.6110^{-14}$	$1.9110^9$	4.0
9	0.93	$2.5810^{-14}$	$2.1610^9$	4.6

(3) interface state density [ $N_{IS}$ ]. The donor density is the property of the ZnO grains, thus it should be the same for any junction in the samples. Our experiment showed that the interface state levels were stable. Thus the interface state density should be responsible for the non-linearity of the junctions. Figure 7 shows the correlation between the non-linearity and the interface state density for single junctions. The junctions with higher interface states density exhibited higher non-linearity. Therefore, it is clear that the  $I$ - $V$  characteristics of single grain boundaries in ZnO varistors are related to the interface state density.

## Conclusion

Properties of single grain boundaries in ZnO:rare-earth varistors were examined by the isothermal capacitance transient spectroscopy (ICTS) method. Single junctions' non-linear exponents obtained by current-voltage measurements varied from 3 to 14. Interface state levels were found to be located at about 0.9 eV below the conduction band edge for every junction. The interface state density of the junctions changed from junction to junction and non-linearity was shown to increase with interface state density.

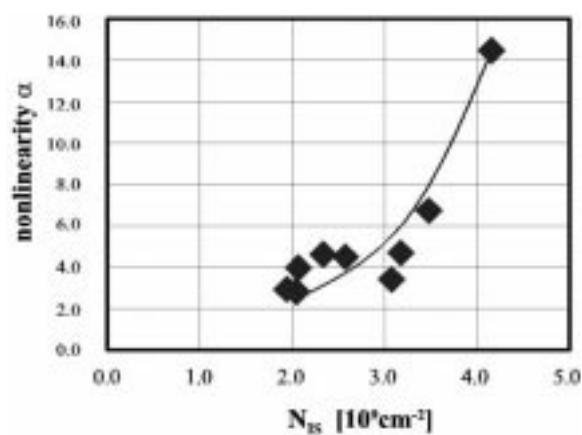


Fig. 7. Correlation between non-linearity and interface state density of single junctions in ZnO varistor.

## Reference

1. M. Matuoka, *Jpn. J. Appl. Phys.*, **10**, 736 (1971).
2. K. Mukae, K. Tsuda, and I. Nagasawa, *Jpn. J. Appl. Phys.*, **16**, 1361 (1977).
3. G. E. Pike, S. R. Kurtz, and P. L. Gourley, *J. Appl. Phys.*, **57**, 5512 (1985).
4. G. D. Mahan, L. M. Levinson, and H. R. Philipp, *J. Appl. Phys.*, **50**, 2799 (1979).
5. K. Mukae and K. Tsuda, *J. Ceram. Soc. Japan*, **100**, 1048 (1992).
6. N. Shohata, T. Matsumura, and T. Ohno, *Jpn. J. Appl. Phys.*, **19**, 1793 (1980).
7. A. Nitayama, H. Sakaki, and T. Ikoma, *Jpn. J. Appl. Phys.*, **19**, L743 (1980).
8. K. Tsuda and K. Mukae, *High Tech Ceramics*, edited by P. Vincenzini (Elsevier, Amsterdam, 1987), pp. 1781.
9. R. A. Winston and J. F. Cordaro, *J. Appl. Phys.*, **68**, 6495 (1990).
10. D. V. Lang, *J. Appl. Phys.*, **45**, 3023 (1974).
11. G. D. Mahan, L. M. Levinson, and H. R. Philipp, *J. Appl. Phys.*, **50**, 2799 (1979).
12. M. Tao, B. Al, O. Dorlante, and A. Loubiere, *J. Appl. Phys.*, **61**, 1562 (1987).
13. J. T. C. Van Kemenade and R. K. Eijthoven, *J. Appl. Phys.*, **50**, 938 (1979).
14. E. Olsson and G. L. Dunlop, *J. Appl. Phys.*, **66**, 3666 (1989).
15. H. Wang, V. Li, and F. Cordaro, *Jpn. J. Appl. Phys.*, **34**, 1765 (1995).
16. H. Okushi and Y. Tokumaru, *Jpn. J. Appl. Phys.*, **19**, L335 (1980).
17. T. Maeda, S. Meguro, and M. Takata, *Jpn. J. Appl. Phys.*, **28**, L714 (1989).
18. K. Tsuda and K. Mukae, *J. Ceram. Soc. Japan*, **100**, 1239 (1992).
19. K. Mukae, K. Tsuda, and I. Nagasawa, *J. Appl. Phys.*, **50**, 4475 (1979).